

Au@Ag Core-shell Nanoparticles Supported on Carbon Nanotubes as Promising Catalysts for Oxygen Electoreduction

Na Li^{1,2}, Changhong Wang^{*,1}, Tingzhen Li^{1,2}, Brendan Latimer³, Zhen Liu³ and Zhenghua Tang^{*,2,4}

¹ School of Materials and Energy, Guangdong University of Technology, Guangzhou, 510006, P. R. China. Email: wangchh@gdut.edu.cn

² Guangzhou Key Laboratory for Surface Chemistry of Energy Materials, New Energy Research Institute, School of Environment and Energy, South China University of Technology, Guangzhou Higher Education Mega Centre, Guangzhou, 510006, P. R. China. Email: zhht@scut.edu.cn

³ Department of Physics & Engineering, Frostburg State University, Frostburg, MD 21532-2303, United States

⁴ Guangdong Provincial Key Laboratory of Atmospheric Environment and Pollution Control, Guangdong Provincial Engineering and Technology Research Center for Environmental Risk Prevention and Emergency Disposal, School of Environment and Energy, South China University of Technology, Guangzhou Higher Education Mega Centre, Guangzhou, 510006, P. R. China

*E-mail: zhht@scut.edu.cn

Received: 16 February 2018 / Accepted: 15 April 2018 / Published: 5 June 2018

Bimetallic nanoparticles with core-shell structure usually demonstrate enhanced catalytic performance due to the lattice strain created between the core and the shell region. The Au@Ag core-shell nanoparticles with different Au-to-Ag molar ratios were firstly fabricated by a facile method under mild conditions, and the n(Au): n(Ag) = 1: 2 sample showed the best electrocatalytic activity toward oxygen reduction reaction (ORR), a key reaction which plays an important role in fuel cells and metal-air batteries. Subsequently, the Au@Ag nanoparticles of n(Au): n(Ag) = 1: 2 were loaded on carbon nanotubes to prepare nanocomposite catalysts with different metal mass ratios of 20% Au@Ag/CNTs, 30% Au@Ag/CNTs, 40% Au@Ag/CNTs, and 50% Au@Ag/CNTs. The characteristics of the as-synthesized nanocomposites were examined by transmission electron microscopy (TEM), X-ray diffraction (XRD) and X-ray photoelectron spectroscopy (XPS) as well. The nanocomposites demonstrated effective electrocatalytic performance toward ORR. Electrochemical tests showed that the 30% Au@Ag/CNTs sample exhibited the highest activity among the series, in aspects of onset potential and kinetic current density. Furthermore, the sample of 30% Au@Ag/CNTs exhibited markedly higher long-term stability than Pt/C. The results clearly illustrate that the Au@Ag core-shell nanoparticles-based nanocomposites hold great potentials as efficient ORR catalysts for fuel cell applications.

Keywords: Au@Ag core-shell nanoparticles; Carbon nanotubes; Nanocomposite catalyst; Oxygen reduction reaction; Fuel cell

1. INTRODUCTION

With the merits of high power density, high energy conversion efficiency, environmental friendliness, and low operating temperature, proton exchange membrane fuel cell (PEMFC) has been gaining tremendous research interests in the past decade, as it holds great potential to resolve the serious environmental pollution issues and global energy crisis.[1-3] One of the crucial limitation factors of PEMFCs to be commercialized is its sluggish oxygen reduction reaction (ORR) occurring at the cathode.[4, 5] Pt and Pt-alloyed nanoparticles integrated with carbon material such as 20 wt% Pt/C have been customarily considered owning the best catalytic activity for ORR; however, the rare Pt reserve on the earth, complicated reaction pathway, and unsatisfactory stability of the Pt-based catalyst significantly restricted its large-scale commercialization of PEMFCs.[6-8] Therefore, substantial research efforts have been devoted to developing cost-effective low-Pt and even non-Pt ORR catalysts with a focus on increasing efficiency and stability to alter the Pt-based catalyst.[8-18]

Among a variety of electrocatalysts for ORR, bi-metallic nanoparticles with core-shell structures usually display enhanced catalytic activity due to the lattice strain created between the core and the shell region.[19, 20] Various bimetallic core-shell structures including Au@Pd,[21] Pd@Pt,[22] Au@Pt,[23] Ir@Pt[24], AuPd@Pd,[25] PdPt@Pd[26] architectures have been prepared. It was observed that these structures demonstrated comparable or even superior ORR activity and durability than benchmark Pt/C catalyst. Au is a unique noble metal that attracts us, as it is chemically inert in the bulk state while excellent electrocatalytic activity can be achieved for the Au nanostructures.[27-31] Furthermore, as its earth abundance is much higher than Pt, Au is slightly cheaper than Pt. Meanwhile, Ag is probably the most economical noble metal in the periodic table. Au alloying Ag with a core-shell structure would be an excellent choice for fabricating non-Pt electrocatalysts, and to the best of our knowledge, rare reports can be found on Au@Ag core-shell structures for ORR to date.

On the other hand, when nanoparticles acting alone as catalysts for electrochemical reaction, they tend to aggregate, decompose or sinter during the electrocatalytic process.[32] To alleviate this issue, a wide range of support materials including graphene,[33] porous carbon,[34, 35] carbon nanosheets,[36] carbon nanotubes[37] as well as other substrates[38] have been extensively utilized to enhance the stability of the nanoparticles. With cylindrical structure imparted unusual physiochemical properties, carbon nanotubes (CNTs) have found a variety of applications in energy storage and conversion.[39, 40] Recently, our lab successfully demonstrated the *in-situ* preparation of multiwall carbon nanotubes entrapped Au nanoclusters for oxygen electroreduction in an alkaline media.[37]

In this study, CNTs supported Au@Ag core-shell nanocomposite catalysts (Au@Ag/CNTs) were prepared. The characteristic of the nanocomposites was examined through XRD, XPS and TEM measurements. The composition of the nanocomposites was fine-tuned by varying the mass ratio of Au@Ag-to-CNTs. The sample of 30% Au@Ag/CNTs demonstrated the best catalytic performance for ORR among a series of samples tested, in the aspects of onset potential and kinetic current density. Moreover, the sample of 30% Au@Ag/CNTs exhibited markedly higher long-term stability than Pt/C.

2. MATERIALS AND METHODS

2.1. Chemicals

Hydrogen tetrachloroauric acid (III) trihydrate ($\text{HAuCl}_4 \cdot 3\text{H}_2\text{O}$, 98%), Bovine serum albumin (BSA), and NaOH were purchased from Energy Chemicals (Shanghai, China), Sodium borohydride (NaBH_4 , 98%) was purchased from Aladdin industrial Corporation (Shanghai, China). Silver nitrate (AgNO_3 , 99%) as well as Pt/C (20 wt %) were purchased from Alfa Aesar (Haverhill Massachusetts). Multiwall carbon nanotubes solution (9-10 wt%, Aladdin industrial Corporation, Shanghai), Water was supplied with a Barnstead nanopure water system ($18.3 \text{ M}\Omega \cdot \text{cm}$). All reagents were used as received.

2.2. Synthesis of Au@Ag core-shell nanoparticles

To prepare Au@Ag core-shell nanoparticles, Au nanoclusters were first synthesized by following a reported procedure.[41] Firstly, the HAuCl_4 solution (5 mL, 10 mM) was added to the BSA solution (5 mL, 50 mg/mL) under vigorous stirring. 2 min later, NaOH solution (0.5 mL, 1 M) was added into the above mixture with vigorous stirring for 12 h at room temperature. The freshly prepared Au nanoclusters (10.5 mL) were then dialyzed by a semi-permeable membrane (molecular weight cutoff = 12k Da) at room temperature. After 24 h and three changes of water at 8 hours intervals, the Au nanoclusters were collected and concentrated.

Next, the Au@Ag core-shell nanoparticles were prepared through a modified procedure in a previous report.[42] The purified Au nanoclusters (10 mL, 5 mM) were first mixed with an aqueous AgNO_3 solution (2.5 mL, 10 mM), and then the NaOH solution (25 μL , 1 M) was introduced immediately. The mixture was kept under vigorous stirring for 24 h at room temperature. The as-synthesized Au@Ag core-shell nanoparticles were dialyzed in semi-permeable membrane tubing (Molecular weight cutoff = 12k Da) for 24 h and the water changed at 8-h intervals, the solution was concentrated and the leftover solid was the Au@Ag core-shell nanoparticles.

2.3. Preparation of the Au@Ag/CNTs Composite

20 mg of CNTs were first dispersed in 20 mL water in a round-bottom flask. Separately, 20 mg of Au@Ag nanoparticles with $n_{\text{Au}}: n_{\text{Ag}} = 1: 2$ were dissolved in 20 mL water under constant stirring for 20 min. The two solutions were mixed in different stoichiometries, and the total metal (Au+Ag) mass ratio of the composite was set as 20%, 30%, 40%, and 50%, while the corresponding sample was denoted as 20% Au@Ag/CNTs, 30% Au@Ag/CNTs, 40% Au@Ag/CNTs and 50% Au@Ag/CNTs, respectively. The mixture was sonicated for 3 hours at room temperature. Finally, the solvents were removed by freeze drying, and the residual solids were the composite catalysts.

2.4. Characterizations

The UV-visible absorbance of Au@Ag core-shell nanoparticles was tested through a Shimadzu 2600/2700 UV-visible scanning spectrophotometer. The microstructure and morphological characteristics of the samples were characterized by high-resolution (HR) TEM (JEOL TEM-2010) with the function of an energy dispersive X-ray spectroscopy (EDS) test. The composition of the samples was analyzed by XPS test through a VG Multi Lab 2000 instrument with a monochromatic Al K α X-ray source (Thermo VG Scientific). The XRD patterns were carried out at room temperature with the Bragg angle (2θ) changes in the scope of 10-90 degrees by using Bruker D8 diffraction and Cu K α radiation ($\lambda = 0.1541$ nm).

2.5. Electrochemical measurements

All electrochemical measurements were carried out on a CHI 750E electrochemical workstation (CH instruments Inc) with a standard three-electrode system in 0.1 M KOH solution at room temperature. The platinum wire electrode worked as the counter electrode and the Ag/AgCl electrode performed as the reference electrode. The working electrode was a glassy carbon-disk electrode (37% collection efficiency, diameter 5.61 mm) from the PINE instruments. The working electrode was cleaned with 0.3 μm alumina powder on a polishing mica cloth in advance.

Typically, the catalyst ink was prepared as the method shown below: 1 mg catalyst was dispersed in 0.5 mL anhydrous ethanol solution with 5 μL 5 wt% Nafion added into the mixture as well. The mixture was then sonicated for at least half an hour to form catalyst ink. 10 μL ink was dropcast onto the glassy carbon electrode and dried at room temperature. The catalyst mass loading of all samples on the electrode surface was 80.8 $\mu\text{g cm}^{-2}$. The cyclic voltammograms (CV) were collected in both O $_2$ and N $_2$ saturated 0.1 M KOH solution with a 10 mV s^{-1} scan rate, and the linear sweep voltammograms (LSV) were conducted in O $_2$ -saturated 0.1 M KOH solution with a scan rate of 10 mV s^{-1} . In all tests, the Ag/AgCl reference electrode was standardized with respect to a reversible hydrogen electrode (RHE). $E_{RHE} = E_{Ag/AgCl} + 0.966$ V. Chronoamperometric responses were recorded at +0.5 V for 30, 000 s in an O $_2$ -saturated 0.1 M KOH solution. Accelerated durability test (ADT) from +0.6 V to +1.0 V at 50 mV s^{-1} with a 900 rpm rotation rate was carried out in O $_2$ -saturated 0.1 M KOH solution before and after 2, 500 cycles of potential scans.

3. RESULTS AND DISCUSSION

3.1. UV-visible absorbance, structural analysis and ORR activity of the Au@Ag core-shell nanoparticles

The UV-visible absorbance spectra of the as-prepared Au nanoclusters and Au@Ag core-shell nanoparticles can be found in Figure S1. For Au nanoclusters alone, the featureless

exponential decay profile can be clearly observed. The absence of characteristic surface plasmon resonance peak around 520 nm from relatively larger Au nanoparticles indicate that, small Au clusters with diameter less than 2 nm were most likely obtained.[31, 43] Interestingly, for the Au@Ag core-shell nanoparticles, there is a broad absorption peak at around 443 nm, a characteristic feature of plasmonic Ag nanostructure.[44] The typical TEM images at different magnifications and homologous size distribution histograms can be found in Figure 1. While closely examining this figure, well-defined spherical particles can be easily identified. The average diameter of the sample was calculated as 4.80 ± 0.53 nm based on no less than 100 individual particles.

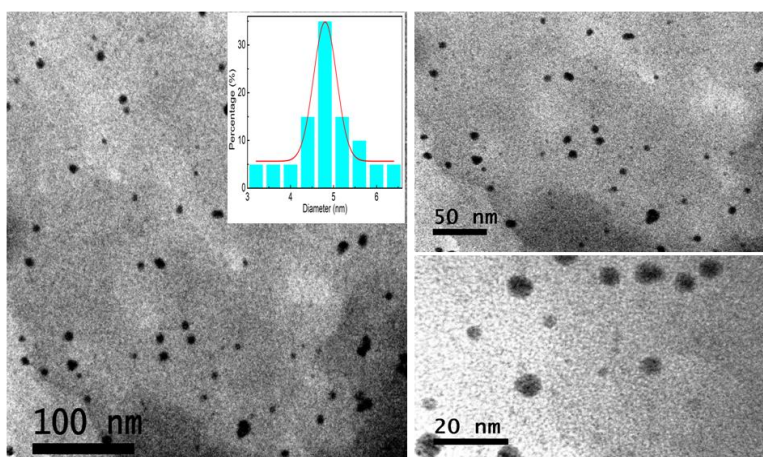


Figure 1. Representative TEM images at different magnifications and corresponding size distribution histogram (inset) of the Au@Ag core-shell nanoparticles.

The electrocatalytic activity toward ORR of the Au@Ag core-shell nanoparticles were then tested. The ORR activity comparison was compiled in Table S1. As illustrated in the cyclic voltammograms in Figure S2a, in O_2 -saturated 0.1 M KOH, a sharp peak between 0.5 and 0.7 V attributed from oxygen reduction can be found for all the samples, indicating valid ORR activity. One may notice that, with the increasing of Ag ratio, the cathodic peak potential and current density first increased then decreased, while the sample of $n_{Au}: n_{Ag} = 1: 2$ exhibited the best ORR performance. This finding was confirmed by the RDE results shown in Figure S2b, as the sample of $n_{Au}: n_{Ag} = 1: 2$ possessed the most positive onset potential (+0.80 V) and the largest kinetic current density (2.56 mA cm^{-2} at 1600 rpm) among the series.

3.2. TEM analysis of Au@Ag/CNTs nanocomposites with different alloy loading

As the Au@Ag core-shell nanoparticle with $n_{Au}: n_{Ag} = 1: 2$ exhibited the best ORR activity, the Au@Ag/CNTs nanocomposites were then prepared by integrating the sample with multiwall carbon nanotubes. Upon the formation of Au@Ag/CNTs nanocomposites, the surface microstructure and morphological characters of all the samples were examined by TEM. The representative TEM images of the hybrid materials and their homologous size distribution

histograms are shown in Figure S3. For the lower metal mass loading samples (20% Au@Ag/CNTs and 30% Au@Ag/CNTs), spherical particles were well dispersed onto the CNTs, and no apparent aggregation can be observed. However, with the increase of metal mass loading (40% Au@Ag/CNTs and 50% Au@Ag/CNTs), the agglomeration phenomenon began to appear, and bulky materials formed particularly for the sample with the metal mass loading of 50% Au@Ag/CNTs. The average diameter of the nanoparticles in the composite was calculated as 4.87 ± 1.49 nm, 15.36 ± 4.15 nm, 38.84 ± 3.12 nm, and 76.7 ± 20.95 nm for the sample of 20% Au@Ag/CNTs, 30% Au@Ag/CNTs, 40% Au@Ag/CNTs, and 50% Au@Ag/CNTs, respectively.

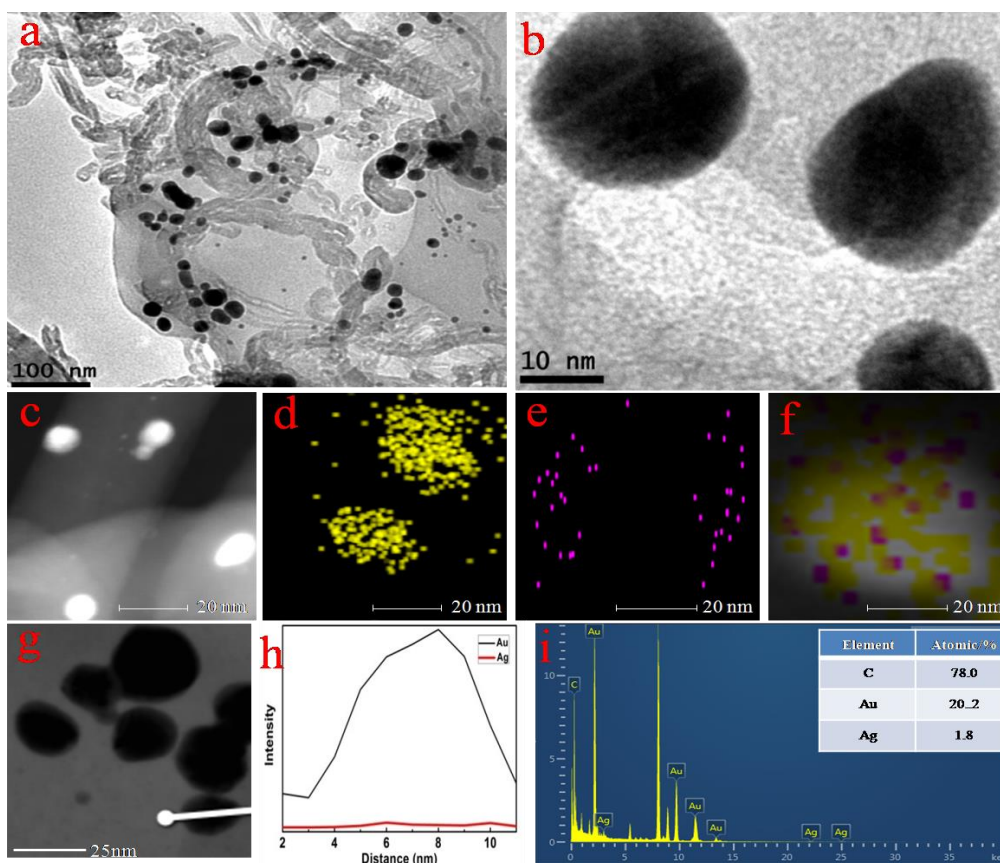


Figure 2. Component and structure characterization of 30% Au@Ag/CNTs. Representative HR-TEM images at 100 nm (a) and 10 nm magnification (b). (c) HAADF-STEM image and EDS mapping images of Au (d), Ag (e) and Au+Ag (f). (h) Line-scan profiles of Au and Ag from the direction marked by a white line in (g). (i) EDX spectrum of Au@Ag/CNTs, and the inserted table displays the elemental content of C, Au, and Ag in Au@Ag/CNTs.

To closely examine the surface structure of the nanocomposite, high-angle annular dark-field scanning transmission electron microscopic (HAADF-STEM) measurements and energy dispersive X-ray spectroscopic (EDS) mapping of the 30% Au@Ag/CNTs were conducted, as shown in Figure 2. From Figures 2a and 2b, well-defined spherical particles with slight aggregation can be observed for 30% Au@Ag/CNTs sample. From the high-magnification EDX images in Figures 2c-f, homogeneous distributions of Au and Ag elements can be

observed, and the atomic ratio of Au-to-Ag was estimated to be 11: 1 (Figure 2i), where a line scan profile (Figure 2g) showed that Ag was at a significantly lower concentration, somewhat enriched at the edges, whereas Au displayed a peak-shaped distribution. These measurements confirm that the Au@Ag core-shell structure on the carbon nanotube was successfully obtained.

3.3. XRD and XPS analysis of samples with different Au@Ag-to-CNTs mass ratios

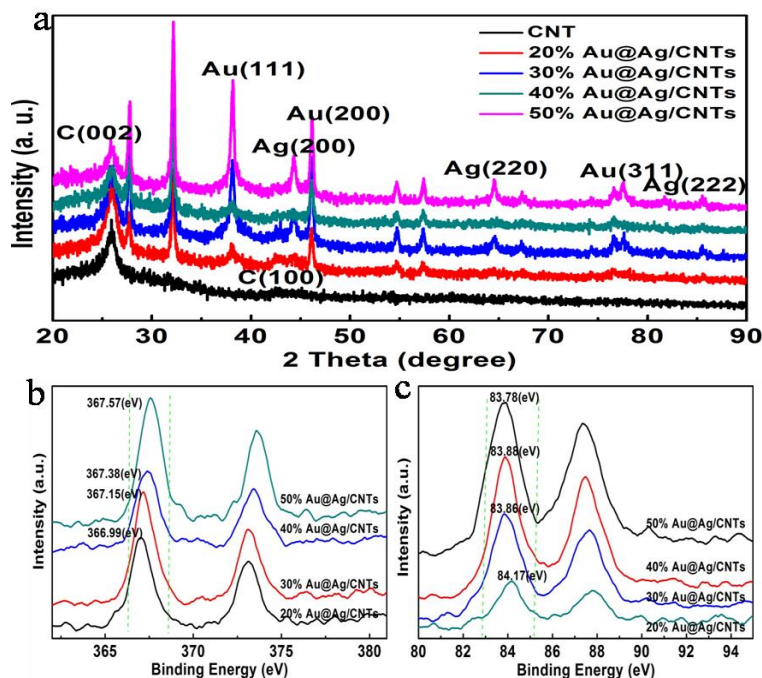


Figure 3. (a) XRD patterns, (b) Ag3d and (c) Au4f core-level spectra of the samples with different metal mass loadings (20% Au@Ag/CNTs, 30% Au@Ag/CNTs, 40% Au@Ag/CNTs, and 50% Au@Ag/CNTs).

The surface structure and composition of the series of nanocomposites were further analyzed by XRD and XPS measurements. From the XRD results in Figure 3a, two diffraction angles of 2θ at 25.9° and 42.6° can be clearly seen, which correspond to C (002) and C (100) crystal planes, respectively. For Au@Ag/CNTs nanocomposites, six additional diffraction peaks can be easily identified at 2θ of 38.1° , 44.2° , 46.2° , 64.5° , 77.6° , and 85.5° , respectively. The six diffraction peaks are in good accordance with the crystal planes of Au (111), Ag (200), Au (200), Ag (220), Au (311), and Ag (222), respectively. The survey scan spectra of XPS can be found in Figure S4, where the strong signals from Au (Au4f, 85.8 eV) and Ag (Ag3d, 367 eV) can be detected in addition to the peaks of C1s (*ca.* 284.5 eV) and O1s (*ca.* 531.9 eV) from carbon nanotubes in the composites. The results further attest that the Au@Ag core-shell nanoparticles have been integrated well with the carbon nanotubes.

The core-level XPS spectra of Ag3d, Au4f and C1s electrons in the composites are shown in Figure 3b, Figure 3c and Figure S5 respectively. It is evident that, with the increasing

of Au@Ag nanoparticle loading, the binding energy of the Ag3d_{5/2} electron increased, while in contrast, the binding energy of the Au4f_{7/2} and C1s electrons decreased. These changes not only suggest the strong electronic interaction between the Au core and the Ag shell, but also indicate that the electron transfer occurred from the Au@Ag core-shell nanoparticles to the CNTs. Note that, such electronic interaction and electron transfer behaviors have been documented to promote the electron transfer kinetics and mass transport activities during the electrocatalytic process.[37, 45]

3.4. ORR performance comparison of the samples with different Au@Ag -to-CNTs ratios

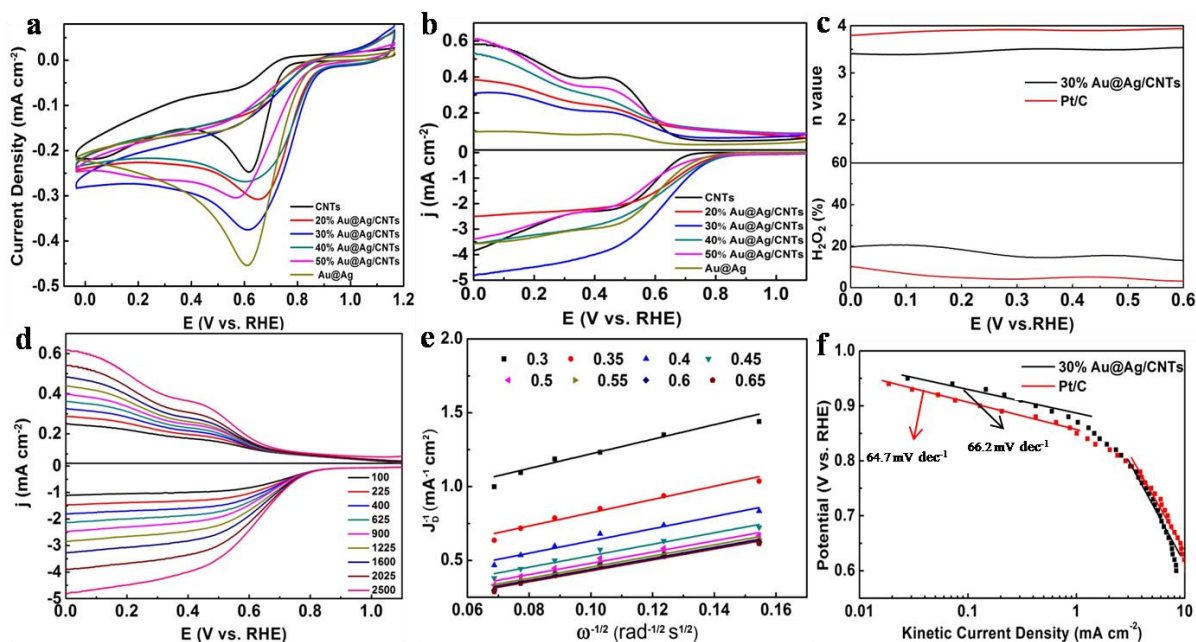


Figure 4. The electrochemical performance of the glassy carbon electrode (GCE) modified with the samples of different Au@Ag-to-CNTs ratios: (a) Cyclic voltammetry, (b) Rotating ring-disk electrode (RRDE) voltammogram, at a rotation speed of 2500 rpm with 10 mV s⁻¹ potential scan rate, (c) Plots of number of electron transfer and H₂O₂ yield (%), (d) Voltammetric current of 30% Au@Ag/CNTs at the rotation rate of 100 to 2500 rpm with 10 mV s⁻¹ potential sweep rate, (e) Corresponding Koutecky–Levich plots of 30% Au@Ag/CNTs composite catalyst at different potentials, (f) Tafel plots of 30% Au@Ag loading and commercial Pt/C. All measurements were performed with a catalyst loading of 80.8 μg cm⁻² in an O₂-saturated 0.1 M KOH aqueous solution at a potential scan rate of 10 mV s⁻¹.

The catalytic activity of the composite catalysts Au@Ag/CNTs toward ORR was then tested by cyclic voltammetry (CV) and rotating ring-disk electrode (RRDE) measurements. In O₂-saturated 0.1 M KOH solution as shown in Figure 4a, all the samples exhibited an evident cathodic peak attributed to oxygen reduction around 0.6 V, indicating valid catalytic activity. However, the composite sample of 30% Au@Ag/CNTs possessed the greatest cathodic peak potential and the largest kinetic current density, superior than Au@Ag core-shell nanoparticle

alone, carbon nanotubes alone and the other samples in the series. Well-agreed results were also achieved from the LSV tests in Figure 4b. The ORR activity comparison of the series is summarized in Table S2. In Figure 4b, the sample of 30% Au@Ag/CNTs presented an onset potential of +0.85 V and a kinetic current density of 4.37 mA cm^{-2} , which are superior to the other samples. Besides, the voltammetric current of the disk electrode has an order of magnitude than that of the ring electrode, indicating that a fairly small amount of hydrogen peroxide was generated during the catalytic process.[45, 46]

It is worth noting that, the catalytic activity varied drastically with the Au@Ag core-shell nanoparticle loading ratio from 20% Au@Ag/CNTs to 50% Au@Ag/CNTs. Principally, the increase of the Au@Ag core-shell nanoparticle loading provided more electrocatalytically active sites, the super electrocatalytic activity of 30% Au@Ag/CNTs than that of 20% Au@Ag/CNTs well demonstrated this view. However, further increase of the mass loading of Au@Ag nanoparticles would lead to agglomeration of the nanoparticles onto the carbon nanotubes, as observed in the TEM images in Figure S3, which reduced the catalytic activity in turn.

Subsequently, the electron transfer number and yield of H_2O_2 can be calculated through the following equations:[47, 48]

$$n = \frac{4I_d}{I_d + I_r / N} \quad (1)$$

$$\text{H}_2\text{O}_2 = \frac{200I_r / N}{\frac{I_r}{N} + I_d} \quad (2)$$

Where I_d represents the disk current of the electrode, I_r represents the ring current of the electrode, and N represents the collecting efficiency (37%) of the electrode. The calculated results for the 30% Au@Ag/CNTs sample and Pt/C can be found in Figure 4c. The n value changed from 3.40 to 3.53 within the potential range from +0.0 V to +0.6 V, while the yield of H_2O_2 varied from 12.0% to 20%, both approaching that of Pt/C ($n = 3.70\text{-}3.86$, H_2O_2 yield = 5.0% - 8.4%). The results imply that the reaction probably adopted a near four-electron transfer pathway and a small amount of intermediate product H_2O_2 was produced during the process.[28, 29, 34, 36, 45]

Figure 4d shows the RRDE results toward ORR for the 30% Au@Ag-CNTs sample recorded with different rotation rates varying from 100 ppm to 2500 ppm. It can be noted that, with the increasing of rotation rate, the voltammetric current increased accordingly. The corresponding Koutecky-Levich (K-L) plots can be found in Figure 4e. A dominant linearity with a rather consistent slope can be recognized, suggesting a first order reaction kinetics of ORR with respect to the oxygen concentration in the solution. Figure 4f displays the corresponding Tafel plots of 30% Au@Ag/CNTs and Pt/C. For the sample of 30% Au@Ag/CNTs, the Tafel slope was calculated as 66.2 mV dec^{-1} , which was quite close to that of commercial Pt/C (64.7 mV dec^{-1}). This closeness in slope suggests that the 30% Au@Ag/CNTs adopted the similar reaction mechanism with that of commercial Pt/C, where

the first electron transfer to molecular oxygen is the rate determining step in the ORR catalytic process.[7, 29, 45, 49]

3.5 Durability comparison of 30% Au@Ag/CNTs and commercial Pt/C

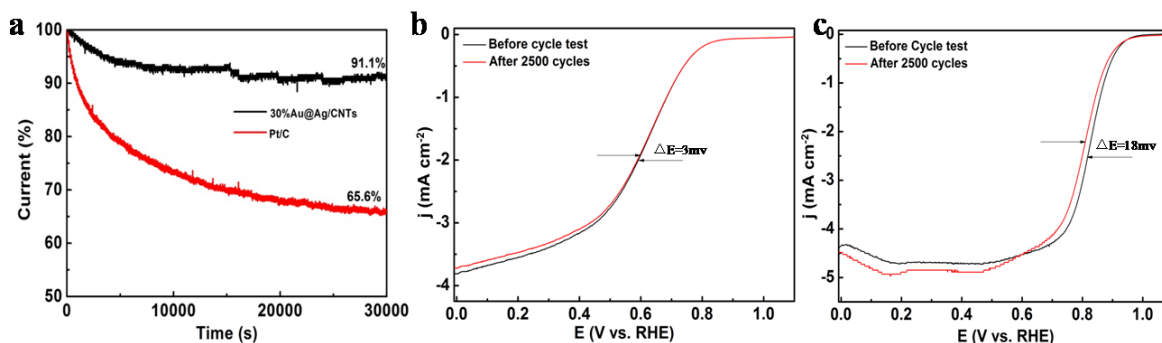


Figure 5. Chronoamperometric responses for ORR at 30% Au@Ag/CNTs and Pt/C electrodes at +0.5 V for 30, 000 s (a), and the polarization curves of the 30% Au@Ag/CNTs (b) and Pt/C (c) before and after 2500 cycles of potential scan. All the measurements were conducted in an O_2 -saturated 0.1 M KOH solution.

Finally, the long-term durability of the 30% Au@Ag/CNTs was measured and compared with commercial Pt/C.[36] Figure 5a shows the chronoamperometric responses for ORR at 30% Au@Ag/CNTs and Pt/C electrodes at +0.5 V for 30, 000 s. It can be seen that, after more than 8 hours' continuous operation, the initial current of the Pt/C electrode dropped to 65.6% (34.4% loss), while in contrast, the starting current of the 30% Au@Ag/CNTs electrode dropped to 91.1% (only 8.9% loss). It suggests that the 30% Au@Ag/CNTs possessed markedly higher stability than that of commercial Pt/C. To further evaluate the stability of the catalysts, accelerate durability tests (ADT) were conducted through cycling the catalyst within the potential range from +0.6 to 1.0 V in an O_2 -saturated 0.1 M KOH solution at 50 mV s^{-1} . [50] As shown in Figure 5b, the half-wave potential of 30% Au@Ag/CNTs only shifted by 3 mV after 2500 cycles of potential scans, while a much larger negative shift of 18 mV was presented by commercial Pt/C (Figure 5c), further confirming remarkable higher durability than commercial Pt/C was acquired for the 30% Au@Ag/CNTs sample.

The ORR performance of the 30% Au@Ag/CNTs sample is at least comparable with some recently documented catalysts, as summarized in **Table S3**. For example, the onset potential was close to that of $\text{Cu}_2\text{ZnSnS}_4\text{-AuAg}$ heterodimers, however 30% Au@Ag/CNTs exhibited much more robust long-term stability than Pt/C, which outperformed than that of $\text{Cu}_2\text{ZnSnS}_4\text{-AuAg}$ heterodimers.[51] In another study, Cao *et al.* prepared Ag@Pt core-shell nanoparticles, although the electrocatalytic performance toward ORR was slightly superior than 30% Au@Ag/CNTs, but the preparation procedure was much more sophisticated and the catalyst was not cost-effective as well. [52]

4. CONCLUSIONS

In this study, we demonstrated the facile preparation of nanocomposites based on Au@Ag core-shell nanoparticles and multiwall carbon nanotubes. The electronic interaction and electron transfer behaviors between the core-shell and carbon nanotubes have been proved to enhance the electron transfer kinetics and mass transport behaviours, both of which can facilitate the electrocatalytic performance of the catalysts. The 30% Au@Ag/CNTs sample demonstrated the greatest activity among the series, in the aspects of onset potential and kinetic current density. More importantly, the long-term durability of the 30% Au@Ag/CNTs sample was markedly higher than that of commercial Pt/C. These findings can shed light on rational design of Au@Ag core-shell nanoparticle-based hybrid materials as efficient electrocatalysts for ORR and beyond.

ACKNOWLEDGEMENTS

This work was supported by the National Natural Science Foundation of China (No. 51676049). Z.H.T acknowledges financial support from Science and Technology Program of Guangdong Province (No. 2017A050506014), Project of Public Interest Research and Capacity Building of Guangdong Province (No. 2015A010105009), Guangdong Innovative and Entrepreneurial Research Team Program (No. 2014ZT05N200), and Guangdong Natural Science Funds for Distinguished Young Scholars (No. 2015A030306006).

SUPPLEMENTARY DATA

Additional ORR activity comparison tables, UV-vis absorbance spectra, CV and RRDE curves of Au@Ag core-shell nanoparticles, additional TEM images, XPS survey scan spectra.

Table S1. The summary of ORR activity of the Au@Ag core-shell nanoparticle samples with different Au-to-Ag molar ratios.

Sample	Molar ratio of Au-to-Ag	E_{onset} (V)	Kinetic current density (mA cm^{-2})
Au@Ag core-shell alloy	2: 1	0.69	1.34
Au@Ag core-shell alloy	1: 1	0.73	2.39
Au@Ag core-shell alloy	1: 2	0.80	3.04
Au@Ag core-shell alloy	1: 3	0.77	1.66

Table S2. The comparison of ORR activity of Au@Ag/CNTs with different metal nanoparticle mass loadings.

Sample	E_{onset} (V)	Kinetic current density (mA cm^{-2})
CNTs	0.72	2.3
20% Au@Ag/CNTs	0.78	2.21

30% Au@Ag/CNTs	0.85	4.37
40% Au@Ag/CNTs	0.80	2.94
50% Au@Ag/CNTs	0.73	2.35
Au@Ag core-shell nanoparticles	0.80	3.04

Table S3. The comparison of ORR activity of Au@Ag/CNTs with different metal nanoparticle mass loadings.

Sample	E_{onset} (V)	Reference
30% Au@Ag/CNTs	0.85	This work
Cu ₂ ZnSnS ₄ -AuAg Heterodimers	0.87	[51]
Carbon-supported Ag@Pt core-shell nanoparticles	About 0.9	[52]

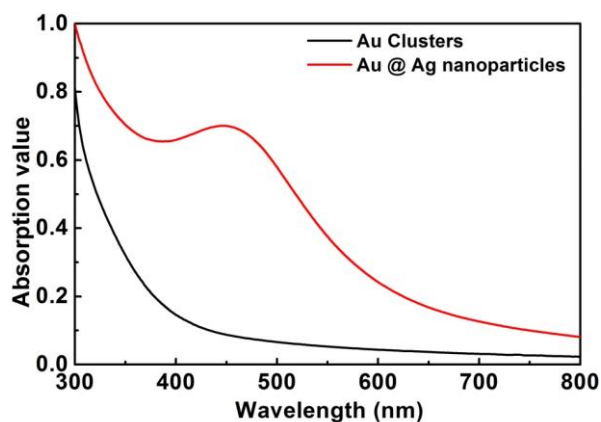


Figure S1. The UV-visible absorbance spectra of the as-prepared Au nanoclusters and Au@Ag nanoparticles.

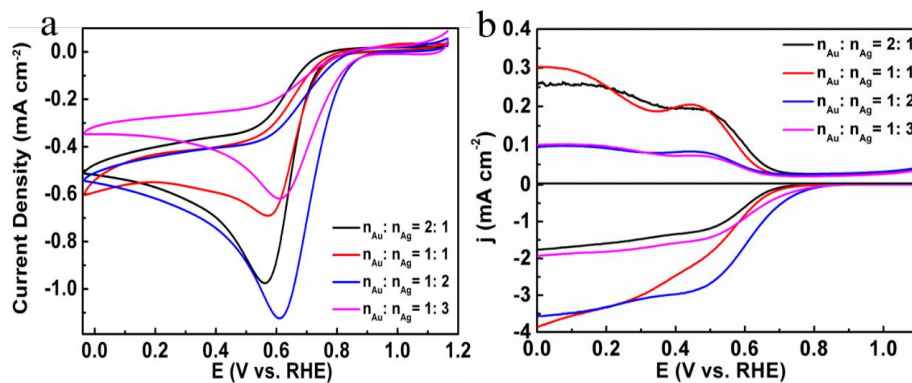


Figure S2. The electrochemical performance of the glassy carbon electrode (GCE) modified with the alloy samples of different Au-to-Ag molar ratios in O₂-saturated 0.1 M KOH solution: (a) Cyclic and (b) Rotating disk electrode (RDE) voltammograms at a rotation speed of 1600 rpm with 10 mV s⁻¹ potential sweep rate.

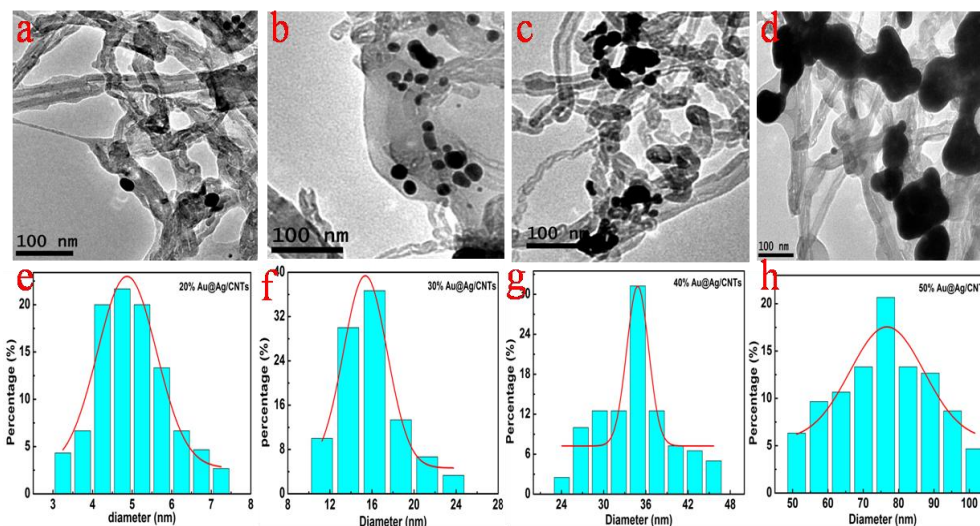


Figure S3. Representative TEM images and corresponding size distribution histograms of 20% Au@Ag/CNTs (a, e), 30% Au@Ag/CNTs (b, f), 40% Au@Ag/CNTs (c, g), and 50% Au@Ag/CNTs (d, h).

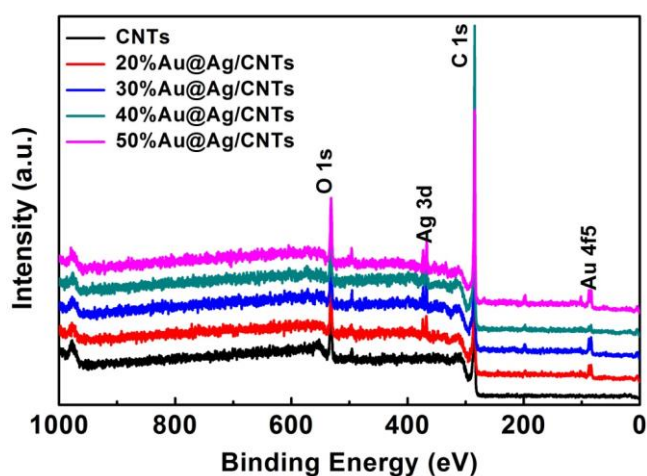


Figure S4. XPS survey scan spectra of the samples with different metal nanoparticle mass loading (20%, 30%, 40% and 50%).

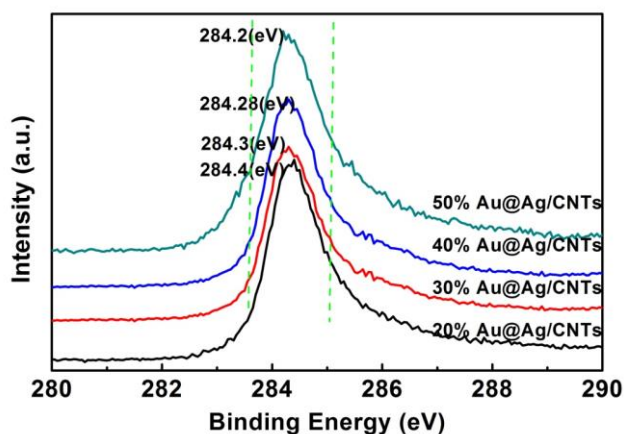


Figure S5. XPS C1s core-level spectra of the nanocomposites with different metal nanoparticle mass loadings.

References

1. S.J. Peighambardoust, S. Rowshanzamir, M. Amjadi, *Int. J. Hydrogen Energy*, 35 (2010) 9349.
2. A. Kraysberg, Y. Ein-Eli, *Energy Fuels*, 28 (2014) 7303.
3. M.K. Debe, *Nature*, 486 (2012) 43.
4. W. Wang, F. Lv, B. Lei, S. Wan, M. Luo, S. Guo, *Adv. Mater.*, 28 (2016) 10117.
5. Z. Tang, W. Wu, K. Wang, *Catalysts*, 8 (2018) 65.
6. H. Osgood, S.V. Devaguptapu, H. Xu, J. Cho, G. Wu, *Nano Today*, 11 (2016) 601.
7. M. Liu, R. Zhang, W. Chen, *Chem. Rev.*, 114 (2014) 5117.
8. M. Shao, Q. Chang, J.-P. Dodelet, R. Chenitz, *Chem. Rev.*, 116 (2016) 3594.
9. W. Wang, B. Lei, S. Guo, *Adv. Energy Mater.*, 6 (2016) 1600236.
10. H. Zhang, H. Osgood, X. Xie, Y. Shao, G. Wu, *Nano Energy*, 31 (2017) 331.
11. W. Ding, L. Li, K. Xiong, Y. Wang, W. Li, Y. Nie, S. Chen, X. Qi, Z. Wei, *J. Am. Chem. Soc.*, 137 (2015) 5414.
12. G. Wu, J. Wang, W. Ding, Y. Nie, L. Li, X. Qi, S. Chen, Z. Wei, *Angew Chem., Int. Ed.*, 55 (2016) 1340.
13. L. Wang, Z. Tang, W. Yan, Q. Wang, H. Yang, S. Chen, *J. Power Sources*, 343 (2017) 458.
14. X. Huang, Z. Zhao, L. Cao, Y. Chen, E. Zhu, Z. Lin, M. Li, A. Yan, A. Zettl, Y.M. Wang, X. Duan, T. Mueller, Y. Huang, *Science*, 348 (2015) 1230.
15. L. Bu, N. Zhang, S. Guo, X. Zhang, J. Li, J. Yao, T. Wu, G. Lu, J.-Y. Ma, D. Su, X. Huang, *Science*, 354 (2016) 1410.
16. L.-L. He, P. Song, A.-J. Wang, J.-N. Zheng, L.-P. Mei, J.-J. Feng, *J. Mater. Chem. A*, 3 (2015) 5352.
17. X.-X. Lin, X.-F. Zhang, A.-J. Wang, K.-M. Fang, J. Yuan, J.-J. Feng, *J. Colloid Interface Sci.*, 499 (2017) 128.
18. C.C. Li, X. Rui, W. Wei, L. Chen, Y. Yu, *Chem. Eur. J.*, 23 (2017) 16242.
19. D. Chen, C. Li, H. Liu, F. Ye, J. Yang, *Sci. Rep.*, 5 (2015) 11949.
20. G. Yang, D. Chen, P. Lv, X. Kong, Y. Sun, Z. Wang, Z. Yuan, H. Liu, *J. Yang, Sci. Rep.*, 6 (2016) 35252.
21. G. Fu, Z. Liu, Y. Chen, J. Lin, Y. Tang, T. Lu, *Nano Res.*, 7 (2014) 1205.
22. L. Zhang, S. Zhu, Q. Chang, D. Su, J. Yue, Z. Du, M. Shao, *ACS Catal.*, 6 (2016) 3428.
23. Y. Dai, S. Chen, *Int. J. Hydrogen Energy*, 41 (2016) 22976.
24. A.L. Strickler, A. Jackson, T.F. Jaramillo, *ACS Energy Lett.*, 2 (2016) 244.
25. J.-N. Zheng, S.-S. Li, X. Ma, F.-Y. Chen, A.-J. Wang, J.-R. Chen, J.-J. Feng, *J. Power Sources*, 262 (2014) 270.
26. J.-J. Lv, J.-N. Zheng, Y.-Y. Wang, A.-J. Wang, L.-L. Chen, J.-J. Feng, *J. Power Sources*, 265 (2014) 231.
27. R.W. Murray, *Chem. Rev.*, 108 (2008).
28. Q. Wang, L. Wang, Z. Tang, F. Wang, W. Yan, H. Yang, W. Zhou, L. Li, X. Kang, S. Chen, *Nanoscale*, 8 (2016) 6629.
29. L. Wang, Z. Tang, W. Yan, H. Yang, Q. Wang, S. Chen, *ACS Appl. Mater. Interfaces*, 8 (2016) 20635.
30. W. Chen, S. Chen, *Angew. Chem., Int. Ed.*, 48 (2009) 4386.
31. S. Wang, H. Yu, M. Zhu, *Sci. China Chem.*, 59 (2016) 206.
32. C. Jeyabharathi, S. Senthil Kumar, G.V.M. Kiruthika, K.L.N. Phani, *Angew. Chem., Int. Ed.*, 49 (2010).
33. C.P. Deming, R. Mercado, V. Gadiraju, S.W. Sweeney, M. Khan, S. Chen, *ACS Sustain. Chem. Eng.*, 3 (2015) 3315.
34. L. Wang, Z. Tang, X. Liu, W. Niu, K. Zhou, H. Yang, W. Zhou, L. Li, S. Chen, *RSC Adv.*, 5 (2015) 103421.
35. H. Geng, J. Yang, H. Yu, C. Li, X. Dong, *Mater. Chem. Front.*, 1 (2017) 1435.

36. W. Yan, Z. Tang, L. Wang, Q. Wang, H. Yang, S. Chen, *Int. J. Hydrogen Energy*, 42 (2017) 218.
37. N. Li, Z. Tang, L. Wang, Q. Wang, W. Yan, H. Yang, S. Chen, C. Wang, *RSC Adv.*, 6 (2016) 91209.
38. C. Lin, Y. Song, L. Cao, S. Chen, *ACS Appl. Mater. Interfaces*, 5 (2013).
39. Q. Wu, L. Yang, X. Wang, Z. Hu, *Acc. Chem. Res.*, 50 (2017) 435.
40. Z. Li, M. Shao, Q. Yang, Y. Tang, M. Wei, D.G. Evans, X. Duan, *Nano Energy*, 37 (2017) 98.
41. S.A. Reilly, T. Krick, A. Dass, *J. Phys. Chem. C*, 114 (2010) 741.
42. J. Xie, Y. Zheng, J.Y. Ying, *Chem. Commun.*, 46 (2010) 961.
43. R. Jin, C. Zeng, M. Zhou, Y. Chen, *Chem. Rev.*, 116 (2016) 10346.
44. J.P. Palafox-Hernandez, Z. Tang, Z.E. Hughes, Y. Li, M.T. Swihart, P.N. Prasad, T.R. Walsh, M.R. Knecht, *Chem. Mater.*, 26 (2014) 4960.
45. Q. Wang, H. Yang, Z. Zhou, L. Wang, W. Yan, W. Wu, S. Chen, Z. Liu, Z. Tang, *Int. J. Hydrogen Energy*, 42 (2017) 11295.
46. D. Li, Z. Tang, S. Chen, Y. Tian, X. Wang, *ChemCatChem*, 9 (2017) 2980.
47. W. Niu, L. Li, X. Liu, N. Wang, J. Liu, W. Zhou, Z. Tang, S. Chen, *J. Am. Chem. Soc.*, 137 (2015).
48. W. Wu, Z. Tang, K. Wang, Z. Liu, L. Li, S. Chen, *Electrochim. Acta*, 260 (2018) 168.
49. C. Wang, N.M. Markovic, V.R. Stamenkovic, *ACS Catal.*, 2 (2012) 891.
50. W. Yan, Z. Tang, L. Li, L. Wang, H. Yang, Q. Wang, W. Wu, S. Chen, *ChemElectroChem*, 4 (2017) 1349.
51. X. Yu, R. Du, B. Li, L. Liu, Y. Zhang, *The J. Phys. Chem. C*, 121 (2017).
52. J. Cao, M. Guo, J. Wu, J. Xu, W. Wang, Z. Chen, *J. Power Sources*, 277 (2015)

© 2018 The Authors. Published by ESG (www.electrochemsci.org). This article is an open access article distributed under the terms and conditions of the Creative Commons Attribution license (<http://creativecommons.org/licenses/by/4.0/>).